Breast imaging with time-reversed ultrasound

Lianjie Huang[a], Nebojsa Duric[b], and Peter Littrup[b]

[a]Los Alamos National Laboratory, Mail Stop D443, Los Alamos, NM 87545
[b]Karmanos Cancer Institute, 4100 John R. Street, 4 HWCRC, Detroit, MI 48201

ABSTRACT

Ultrasonic imaging has the potential to enhance our capability to detect and diagnose breast cancers, but its imaging quality and resolution need to be significantly improved. We make use of the principle of the time-reversal mirror to develop an image-reconstruction method for ultrasonic breast imaging. It reconstructs images of scatterers (e.g., tumors) that generate/scatter ultrasonic waves by backpropagating measured ultrasonic signals into a heterogeneous breast model on computers using the principle of time-reversal mirror. We use solutions of the (two-way) full wave equation and one-way wave equation in heterogeneous media for backpropagation. We found that the one-way wave-equation-based imaging method can produce higher-resolution images than the two-way propagation-based imaging method when the data acquisition aperture is limited (for a linear transducer array). With a full aperture, our imaging results demonstrate that imaging with time-reversed ultrasound can produce high-quality images of the breast.

Keywords: Backpropagation, breast imaging, time-reversed mirror, time-reversed ultrasound, tomography, wave equation.

1. INTRODUCTION

Ultrasound tomography has the potential to interpret measured ultrasonic data with the goal of detecting and diagnosing breast cancer. A number of investigators have been developing tomography-based ultrasound scanners. After the pioneering work of Greenleaf in tissue characterization,[1] a great deal of research on ultrasound tomography has been conducted by many investigators.[2–4] Current work on ultrasound tomography is being carried out on a number of fronts and includes Johnson et al.[5] (TechniScan Inc), Marmarelis' group at USC,[6] Waag's group at Rochester,[7] and a research team associated with the Karmanos Cancer Institute.[8–15] Although the computational and data-acquisition limitations have been major barriers to effective applications of ultrasound tomography, recent technological advances in computing and electronics have led to renewed optimism for the development of clinically relevant tomography-based ultrasound scanners.

The time-reversal mirror (TRM)[16] is an emerging technology that focuses measured ultrasonic signals back to their origins/scatterers in heterogeneous media. It has the potential to dramatically improve breast-imaging capability. The TRM is based on time-reversal (TR) invariance inherent in wave propagation. It has been used for focusing sound in rooms,[17] noncurrent underwater communications,[18] and ultrasonic nondestructive testing,[19,20] etc. It has also been used to focus measured ultrasonic signals back to scatterers like cancers and kidney stones for medical purposes.[21] In current TRM applications, the time-reversed signals are reemitted from receiving transducers to focus them back to the their origins/scatterers.[22,23] However, we still do not know where the scatterers are located and what they are by focusing ultrasound, which are very important for cancer imaging and diagnosis.

We develop a novel breast imaging method by making use of the physics of time-reversal invariance in ultrasonic-wave propagation to "reemit" or backpropagate the time-reversed ultrasound on computers using a sound-speed structure obtained from ultrasound tomography. Ultrasonic-wave propagation is governed by the (full) acoustic-wave equation in heterogeneous media, which describes wave propagation along both forward and backward directions. The full wave equation can be decomposed into two one-way wave equations: one describes forward wave propagation and another describes the backward wave propagation. Hence, the full wave equation is also termed two-way wave equation. We carry out the "reemission" or backpropagation process using solutions of the full acoustic-wave equation or one-way wave equation to focus ultrasonic signals back to scatterers in order to obtain breast images. Ultrasonic transmission tomographic images provide smoothed breast images. By contrast, the new imaging method has the potential to produce tomographic images of lesion shapes, texture and even microcalcifications.

Our long-term goal is to explore the capability of time-reversal imaging in providing high-resolution reflection images from data obtained with ultrasound scanners. As a first step toward that goal, we investigate time-reversal imaging using

Medical Imaging 2006: Ultrasonic Imaging and Signal Processing
edited by Stanislav Emelianov, William F. Walker, Proc. of SPIE
Vol. 6147, 61470I, (2006) 1605-7422/06/$15 · doi: 10.1117/12.659845

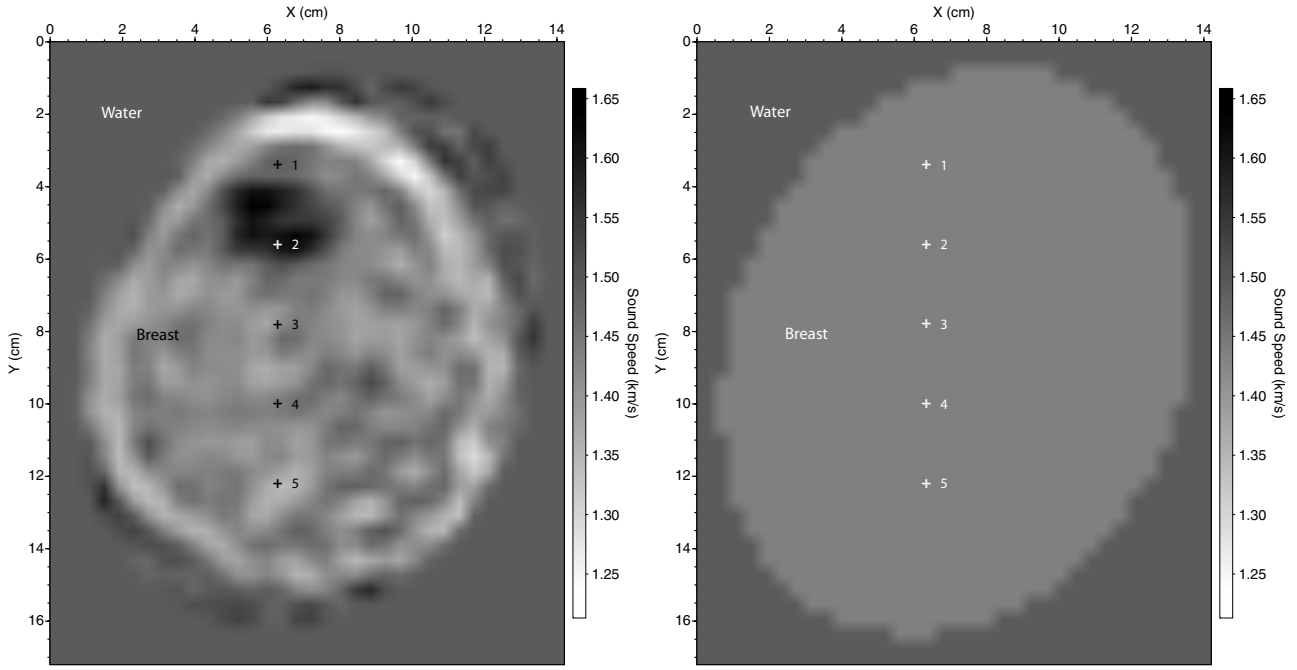

(a) A sound speed model of the breast

(b) An average sound speed model of the breast

Figure 1. (a) A breast sound-speed model obtained from ultrasound tomography of an *in-vivo* dataset. (b) A breast sound-speed model with a constant sound-speed within the breast. The constant sound-speed in (b) is the average sound-speed within the breast in (a).

synthetic data from a numerically defined breast model. Simulated breast masses are inserted into the breast model whose sound speeds were obtained by ultrasound transmission tomography of an actual *in-vivo* dataset acquired at the Karmanos cancer Institute. In this paper, we investigate imaging capability of the our time-reversal imaging method using synthetic data from the heterogeneous breast model. We compare images obtained using different backpropagation approaches and different data-acquisition apertures and demonstrate that high-quality breast images can be obtained using our new imaging method. We discover that imaging with a solution of the one-way wave equation can produce higher-resolution images than those obtained using a solution of the two-way wave equation when the illumination aperture (or the length of a linear ultrasound transducer array) is limited. In addition, we show that breast images can contain significant artifacts if a homogeneous sound-speed model is used for imaging. Therefore, an ultrasonic imaging method capable of properly handling the heterogeneous nature of the breast tissue is critical to the detection of small cancers.

2. TIME-REVERSAL-INDUCED ULTRASONIC WAVES

Sound speeds and densities of breast tissue vary in space, and those of lesions are different from the surrounding tissues. These differences in mechanical properties cause scattering of ultrasonic waves. The sound speed and density of microcalcifications are significantly higher than those of breast tissue, resulting in strong scattering.

When the time-reversed ultrasonic signals are reemitted from the receiving transducers, they will be focused back to the their origins/scatterers. Before reemission, a "mirror" of the time variable is introduced into the recorded signals, and the time axis becomes negative. That is, the time sample of a signal at the maximum time $t_{\max}$ becomes the sample at $-t_{\max}$, and the resulting mirror signals are called time-reversed signals. The time samples at $-t_{\max}$ in the time-reversed signals are reemitted first from the receiving transducers, followed by the next samples at $-t_{\max}+\Delta t$ and so on, until time zero, where Δt is the time sample interval.

At time zero, all signals are focused back to the scatterers if the transmitting/receiving transducers reemitted signals with one half of their original sample interval. The scatterers will then act as secondary sources (or exploding reflectors) to scatter ultrasonic waves again. We refer to the resulting ultrasonic scattering waves as time-reversal-induced (TR-induced) ultrasonic waves. The TR-induced ultrasonic signals recorded again by the receiving transducers will have better

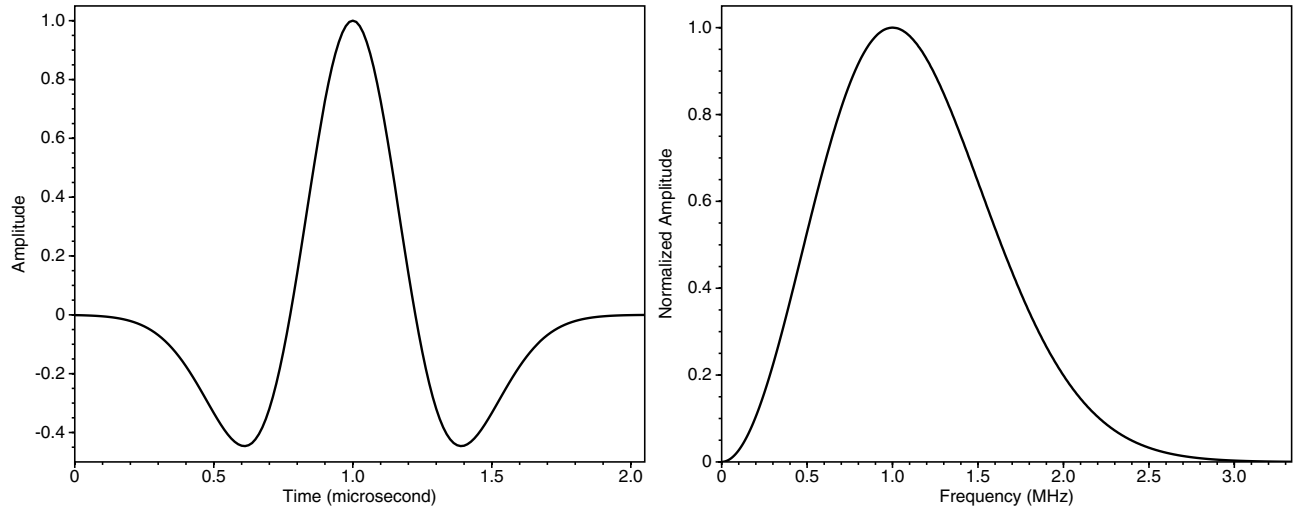

(a) Source-time function (b) Spectrum

Figure 2. (a) The source-time function of a Ricker wavelet with a peak at 1 ms and a central frequency of 1 MHz. (b) Spectrum of the Ricker source-time function in (a).

signal/noise ratios than the original scattering signals and consequently, imaging using the TR-induced signals will enhance image quality.

The concept of exploding-reflector data introduced in seismic imaging more than two decades ago[24] is similar to that of the TR-induced data, but no real exploding-reflector data have been able to be generated because TRM still cannot be applied to seismic data. Using the TRM to focus ultrasound back to scatterers, it is the first time ever to be able to produce TR-induced ultrasonic data, which is the real "exploding-reflector data."

3. ULTRASONIC-WAVE PROPAGATION IN THE BREAST

Ultrasonic-wave propagation in breast tissue is governed by the acoustic-wave equation in heterogeneous media. We used a heterogeneous breast model to simulate ultrasonic-wave propagation using a finite-difference wave-equation scheme, record synthetic signals along the boundaries of the model, and backpropagate the time-reversed ultrasonic signals from the receiving points into the breast model for the imaging purpose.

We conducted a bilinear interpolation of a breast sound-speed model of a preliminary ultrasonic tomography result using a large grid-spacing of 4.072 mm. Figure 1(a) is an interpolated breast sound-speed model with a grid spacing of 0.1 mm. The original tomographic sound-speed model of the breast was obtained from an *in-vivo* dataset collected using Karmanos Cancer Institute's clinical prototype of a ring-transducer array by immersing the breast into water. The sound speed of the breast varies from around 1.3 km/s to around 1.6 km/s, with a region around (x, y) = (6.5 cm, 5 cm) having highest sound speeds. Figure 1(b) is the corresponding breast model with an average sound-speed of 1434.6 m/s within the breast.

We selected five points within the breast model as indicated by "+" signs in Figure 1(a) to introduce ultrasonic sources for forward wave modeling, simulating TR-induced ultrasonic-wave propagation. Point No.1 was located between the low-sound-speed region and the high-sound-speed region, and point No. 2 was located within the high-sound-speed region. The distance between one point to its adjacent one is the same for all the five points in Figure 1(a). A source-time function of the second derivative of a Gaussian function (Ricker wavelet) with a central frequency of 1 MHz (Figure 2) was introduced at each of the five locations. The source-time function has a peak at 1 ms (Figure 2a), and it spectrum has a peak at 1 MHz (Figure 2b). A relative low frequency was used for the convenience of finite-difference calculations. The ultrasonic wavelength within the breast model in Figure 1(a) ranges from 1.3 mm to 1.6 mm.

A finite-difference scheme with a fourth-order accuracy in space and second-order accuracy in time was used for both forward modeling and backpropagation of ultrasonic waves.[25] A Higdon's absorbing boundary condition was used at the boundaries of the model in order to eliminate artificial reflections from the boundaries of the model.[26] Ultrasonic-wave

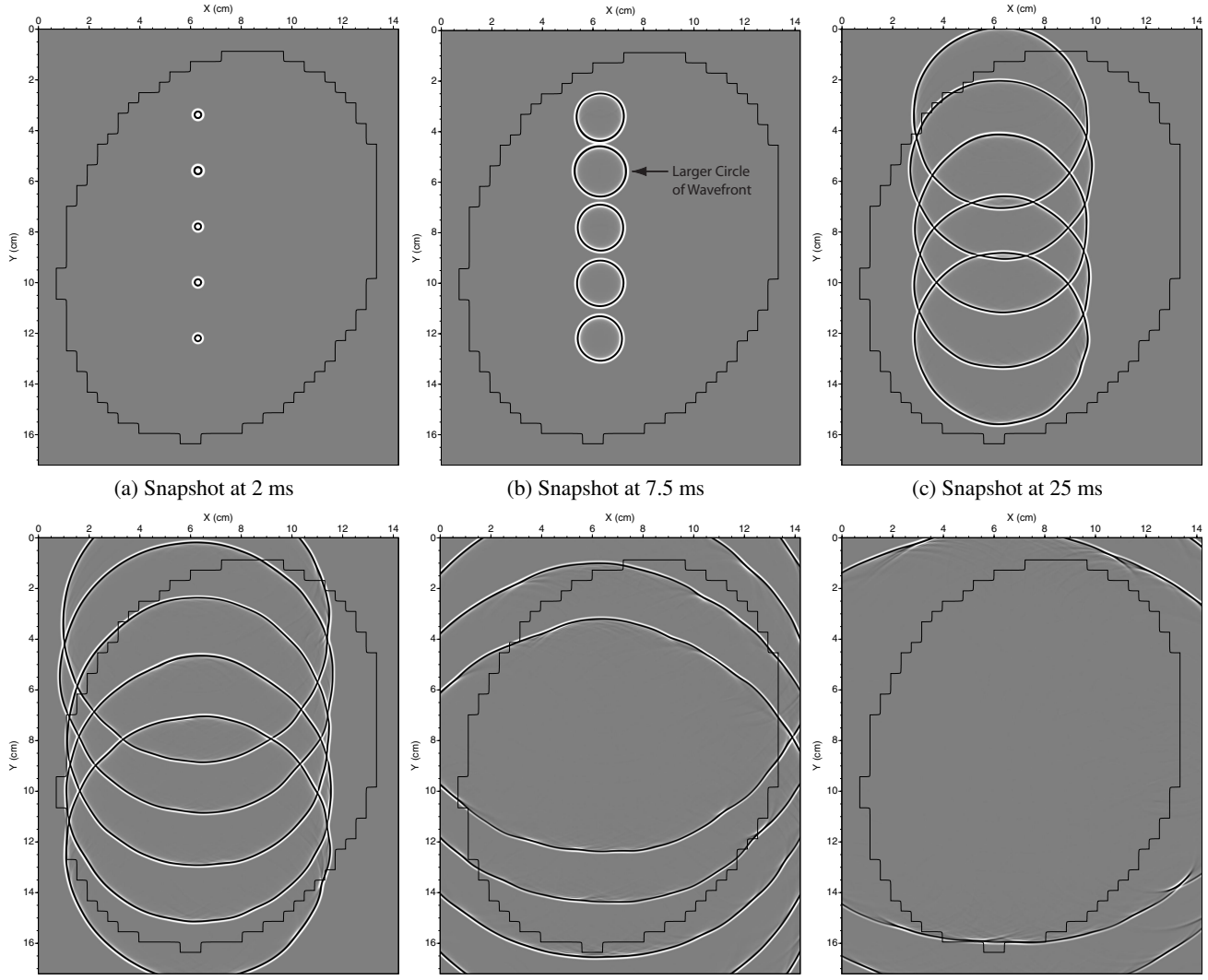

(a) Snapshot at 2 ms (b) Snapshot at 7.5 ms (c) Snapshot at 25 ms

(d) Snapshot at 37.5 ms (e) Snapshot at 62.5 ms (f) Snapshot at 87.5 ms

Figure 3. Snapshots of ultrasonic-wave propagation from the five point sources located within the breast model in Figure 1 demonstrate wavefront distortion and scattering by heterogeneities of the breast. The solid line in each panel indicates the location of the breast. Note that the larger circle indicated by the arrow in (b) is due to the higher-sound-speed tissue around that region.

propagation from the point sources to all boundaries of the breast model in Figure 1(a) is analogous to propagation of TR-induced ultrasonic waves. It is also analogous to an ultrasound system in which each ultrasound transducer located along the square boundary emits ultrasound and records signals scattered from the five point scatterers. The only difference is that the travel times for the this case are twice of those of TR-induced ultrasonic signals.

The snapshots in Figure 3 obtained during the finite-difference modeling demonstrate the effects of heterogeneities within the breast on ultrasonic-wave propagation. The (close) solid line in each panel of Figure 3 shows where the breast was located. Figure 3(a) displayed a snapshot when the entire source-time function was introduced into the breast model. Figure 3(b) shows that the size of the second-from-the-top circle of snapshots is larger than the others due to higher sound-speeds within that region. The wavefronts in Figure 3(c) are no longer circular due to distortion by heterogeneities of the breast, and Figures 3(d-f) demonstrate further distortion of wavefronts and scattering effects during propagation.

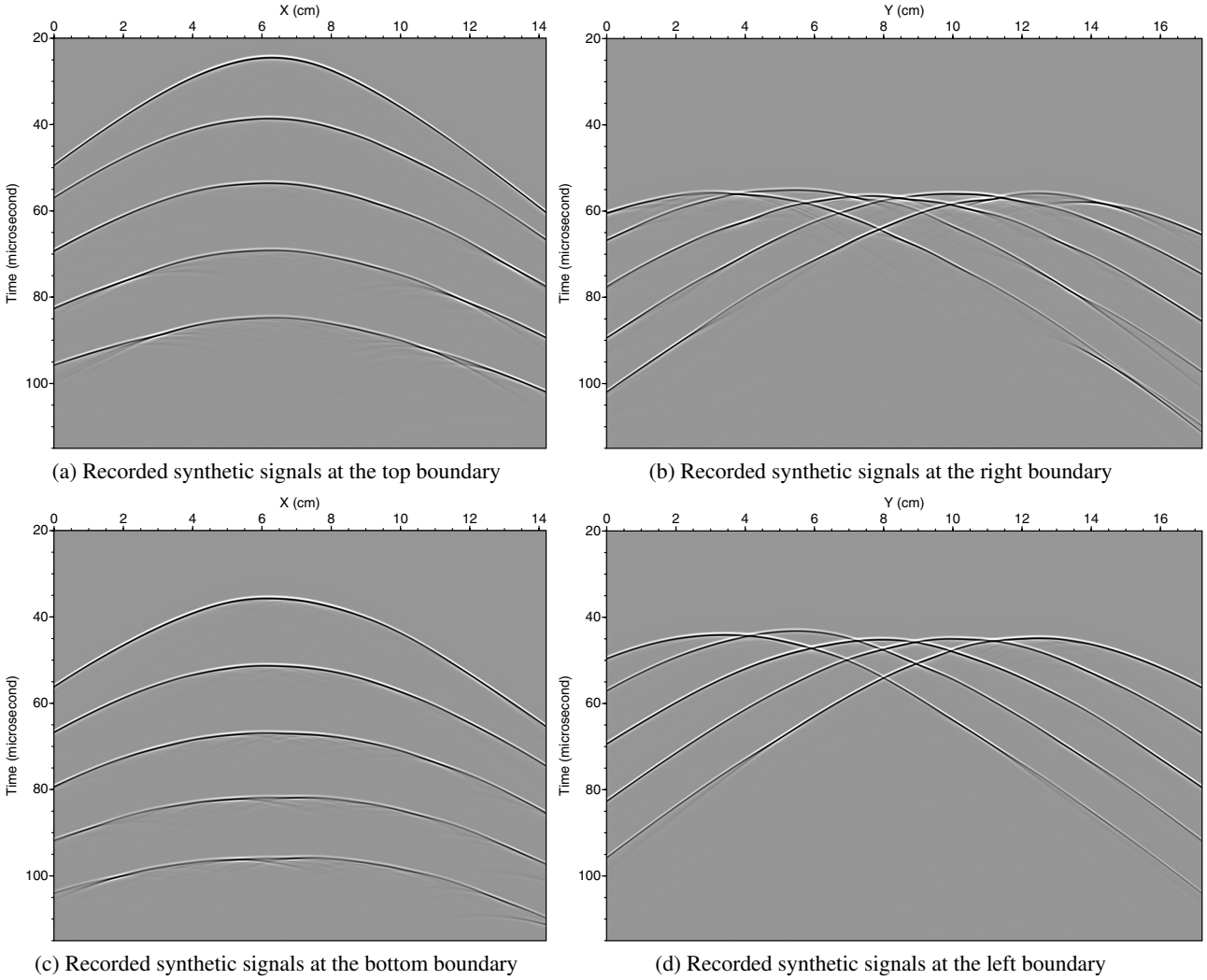

(a) Recorded synthetic signals at the top boundary

(b) Recorded synthetic signals at the right boundary

(c) Recorded synthetic signals at the bottom boundary

(d) Recorded synthetic signals at the left boundary

Figure 4. Synthetic ultrasound signals recorded at the top (a), right (b), bottom (c), and left (d) boundaries of the breast model (Figure 1a). They were used to propagating them back to the locations of the five point sources introduced into the breast model in Figure 1(a).

4. IMAGING WITH TIME-REVERSED ULTRASOUND

Figure 4 depicts the synthetic ultrasound signals recorded along all boundaries of the breast model in Figure 1(a). We backpropagated these TR-induced synthetic signals into the breast model using the finite-difference wave-equation scheme. First we introduced a "mirror" of the time variable to the recorded signals, that is, we turned the time axis upside down in each panel of Figure 4 so that the time axis becomes negative. The resulting signals are called time-reversed signals. Then we used those time-reversed ultrasonic signals as input wavefields at locations where they were recorded during the finite-differencing wave-equation modeling. The time-reversed signals corresponding to the maximum time in each panel of Figure 4 were input first during the finite-difference calculation for the backpropagation of the recorded wavefields. The calculations were conducted until the time axis reaches to zero. Figure 5 shows snapshots of this backpropagation process, illustrating that the wavefronts focused back to their origins — the locations of the five point sources. Some numerical artifacts in the snapshots seen as refracting lines emanating from the rings are caused by the four rectangular corners of the breast model. This indicates that smooth corners might need to be used in TRM experiments.

During the backpropagation of time-reversed signals, the images of the five point sources were obtained when the peak of the source-time function reached the locations of the five points in Figure 1(a). The peak of the source-time function used during forward modeling was at 1 ms (see Figure 2a). Therefore, the images of the five point sources shown in

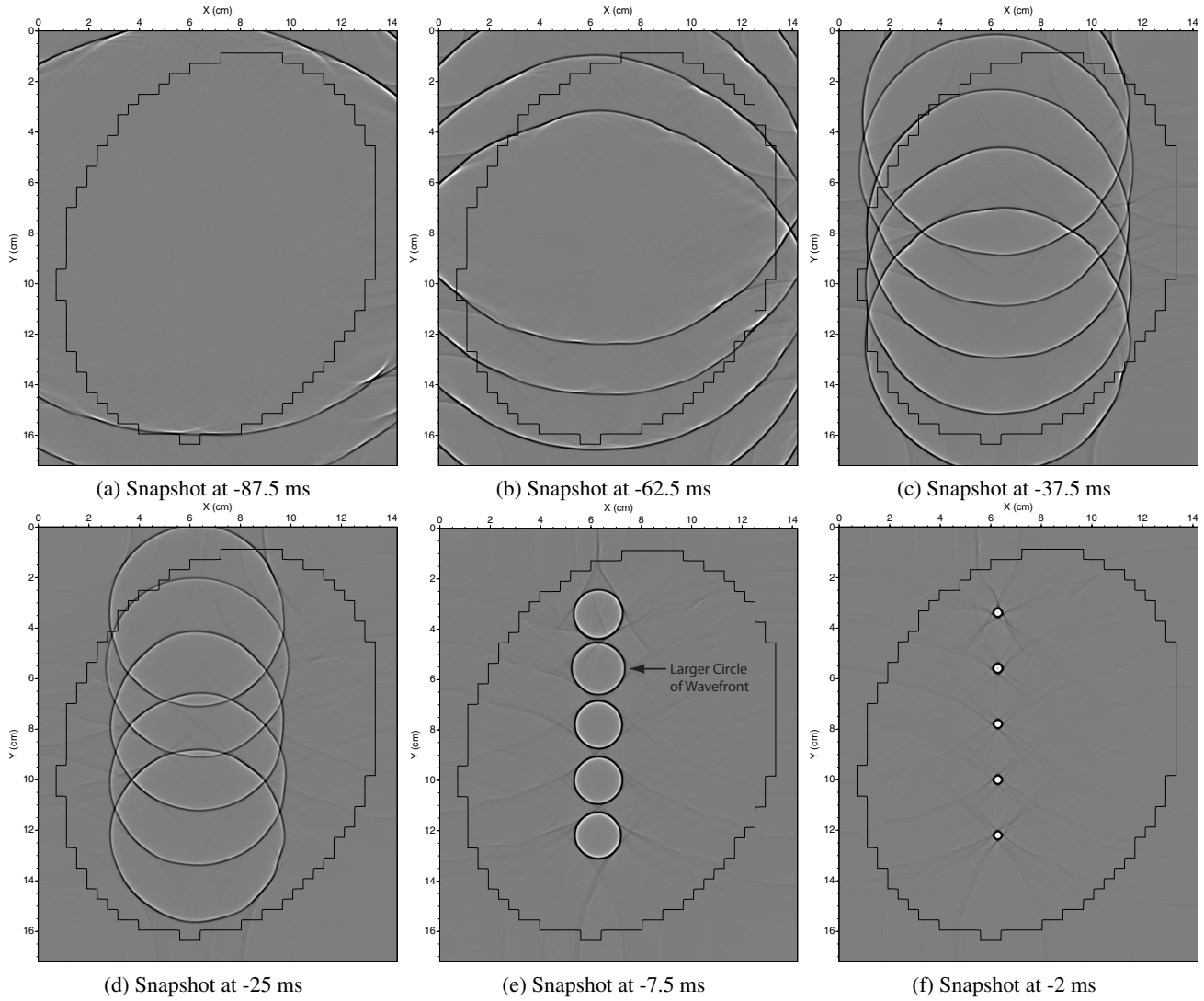

(a) Snapshot at -87.5 ms (b) Snapshot at -62.5 ms (c) Snapshot at -37.5 ms

(d) Snapshot at -25 ms (e) Snapshot at -7.5 ms (f) Snapshot at -2 ms

Figure 5. Snapshots showing the backpropagation process of time-reversed ultrasonic wavefields. The time-reversed ultrasonic signals propagated back to their origins, a process opposite to that in Figure 3. The solid line in each panel indicates the location of the breast. Note that, like Figure 3(b), the larger circle indicated by the arrow in (e) is due to the higher-sound-speeds tissue around that region.

Figure 6(a) were obtained when the time reached -1 ms during the backpropagation calculations. The images of the point sources in Figure 6(a) were obtained with a full aperture, that is, they were produced using all wavefields in Figure 4 that backpropagated from all 360° surrounding the imaging objects. For this case, each image of the point source in Figure 6(a) has the highest resolution and quality.

The illumination apertures at imaging points are limited when using a linear transducer array. We obtained the images of the five point sources using only time-reversed synthetic signals at the top boundary of the breast model in Figure 1 during the backpropagation calculations using the finite-difference (two-way) wave-equation scheme. The resulting images of the five point sources are displayed in Figure 6(b). They contain some image artifacts due to the limited aperture. The image resolution along the x-direction decreases with increasing distance between the point sources and the top boundary of the breast model. The computational time for the two-way wave-equation-based imaging was approximately 51 minutes on a 3.6 GHz PC.

Using only the recorded signals at the top boundary of the breast model, we also conducted backpropagation calculations during imaging using a solution of one-way wave equation in heterogeneous media.[27] The resulting images of the

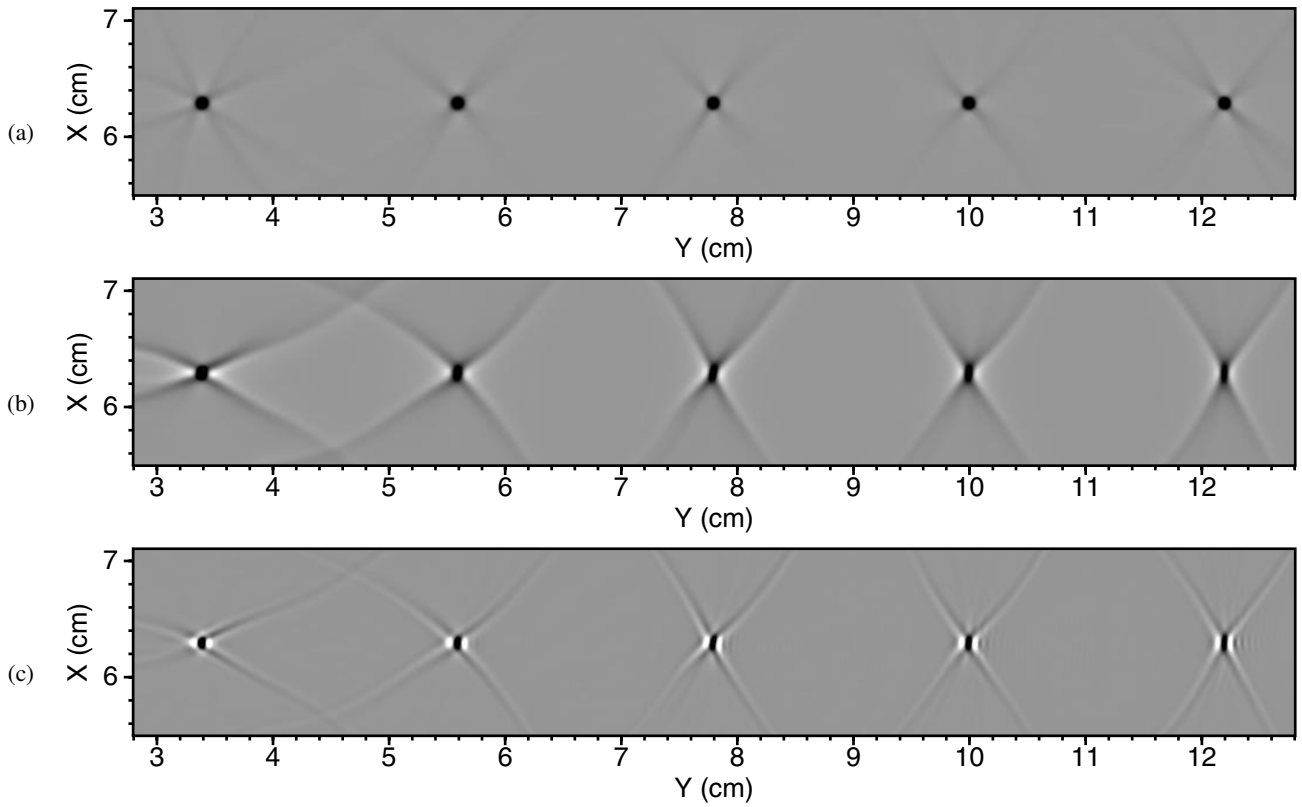

Figure 6. Images in (a) and (b) are imaging results of five point sources obtained by backpropagating time-reversed signals using a finite-difference two-way wave-equation method. (a) is the result when using recorded ultrasonic signals at all boundaries of the breast model, and (b) is that when using only ultrasonic signal at the top boundary of the breast model. (c) is the imaging result yielded using a solution of one-way wave equation for backpropagation of time-reversed data at the top boundary of the breast model.

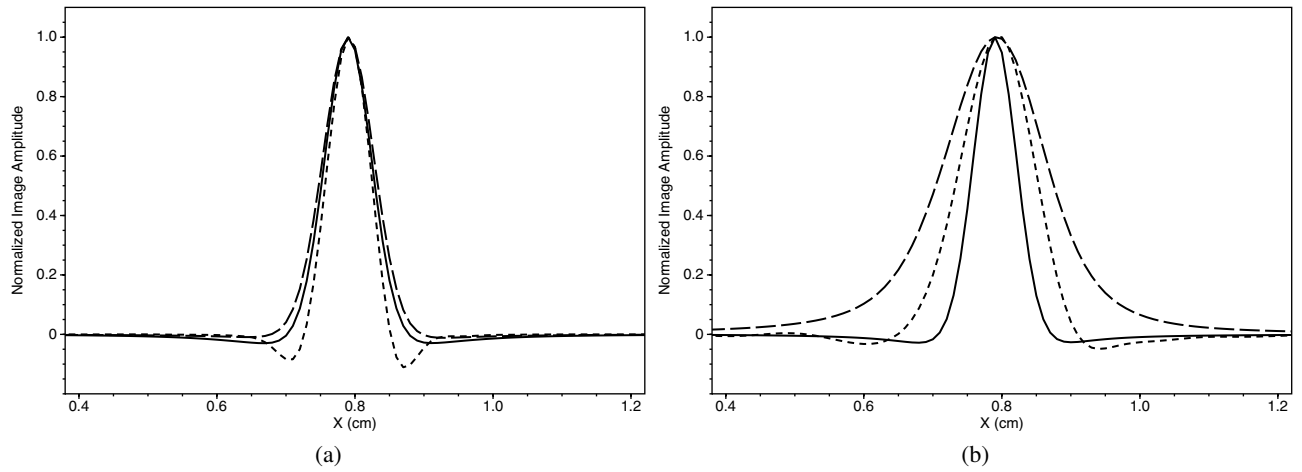

Figure 7. Comparison of normalized images along x-direction shown in Figure 6. The origin of x-axis in each panel corresponds to the minimum value of x-axis in each panel of Figure 6. (a) is for the images of point source No.1 located at y=3.39 cm (cf. Figure 1). (b) is for the images of point source No.5 located at y=12.19 cm (cf. Figure 1). The solid line in each panel is for the image shown in Figure 6(a), the long-dashed-line is for the image shown in Figure 6(b), and the short-dashed-line is for the image in Figure 6(c). The narrower full-width half-maximum provides better image resolution.

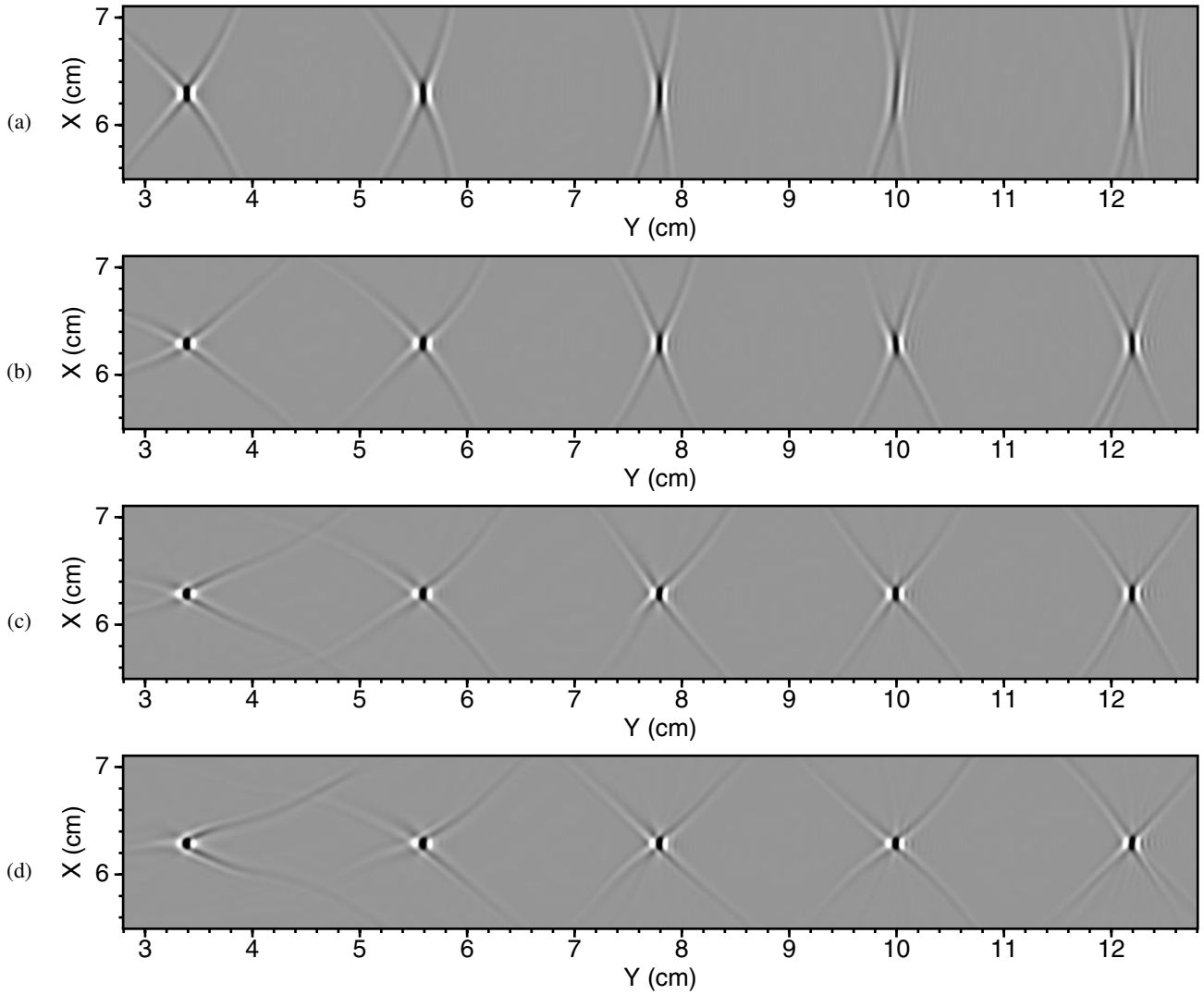

Figure 8. Comparison of images of the five point sources reconstructed using different lengths of linear transducer arrays: (a) 5 cm, (b) 10 cm, (c) 15 cm, (d) 20 cm. Image resolution along x-direction increases with increasing of the transducer array length.

five point sources displayed in Figure 6(c) contain similar artifacts as those in Figure 6(b) due to limited aperture. The computational time for the one-way wave-equation-based imaging was approximately 3 minutes on a 3.6 GHz PC, which is more than 15 times faster than the two-way wave-equation-based imaging.

Figure 7 shows comparisons of normalized images along x-direction for different images in Figure 6. The narrower full-width half-maximum (FWHM) of an image is, the better is the image resolution. When the imaging object is close to a data-acquisition line as shown in Figure 7(a), the image resolution along x-direction for different imaging approaches is similar to one another. However, for the case of limited-aperture imaging, Figure 7(b) demonstrates that the one-way wave-equation-based imaging (short-dashed-line) produced better image resolution than the two-way wave-equation-based imaging (long-dashed-line). A possible explanation of this feature is the following. Two-way (full) wave-equation-based method accounts for ultrasonic waves propagating along all directions and they are not coherently interfered when not using full-aperture data, resulting in stronger artifacts on images than one-way wave-equation-based method, which accounts only for inward propagating waves.

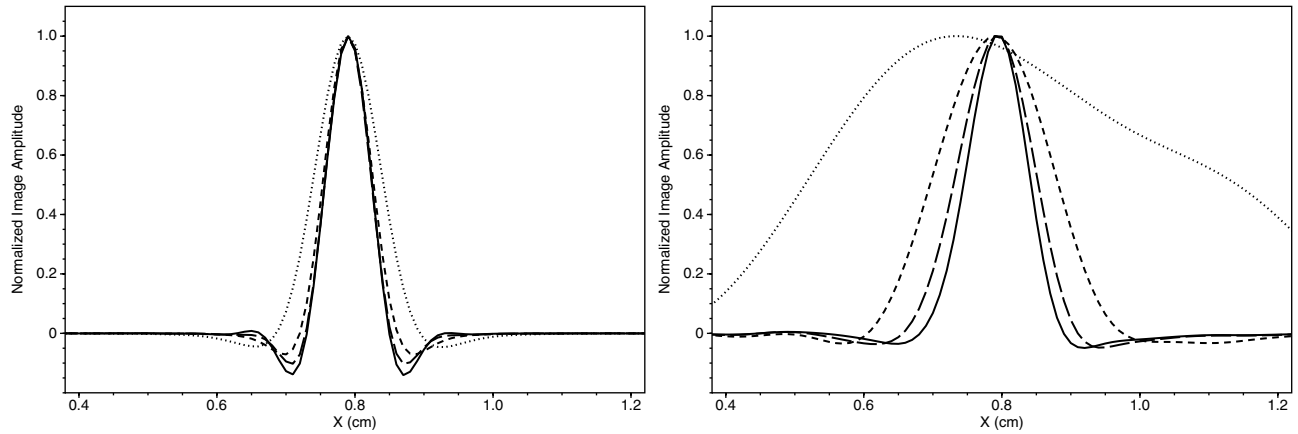

Figure 9. Comparison of normalized images along x-direction shown in Figure 8, showing better resolution for longer transducer-array lengths. The origin of x-axis in each panel corresponds to the minimum value of x-axis in each panel of Figure 8. (a) is for the images of point source No.1 located at y=3.39 cm (cf. Figure 1a). (b) is for the images of point source No.5 located at y=12.19 cm (cf. Figure 1a). The solid line in each panel is for the data length (or length of a linear transducer array) of 20 cm, the long-dashed-line is for the data length of 15 cm, the short-dashed-line is for the data length of 10 cm, and the dotted line is for the data length of 5 cm. The narrower full-width half-maximum provides better image resolution.

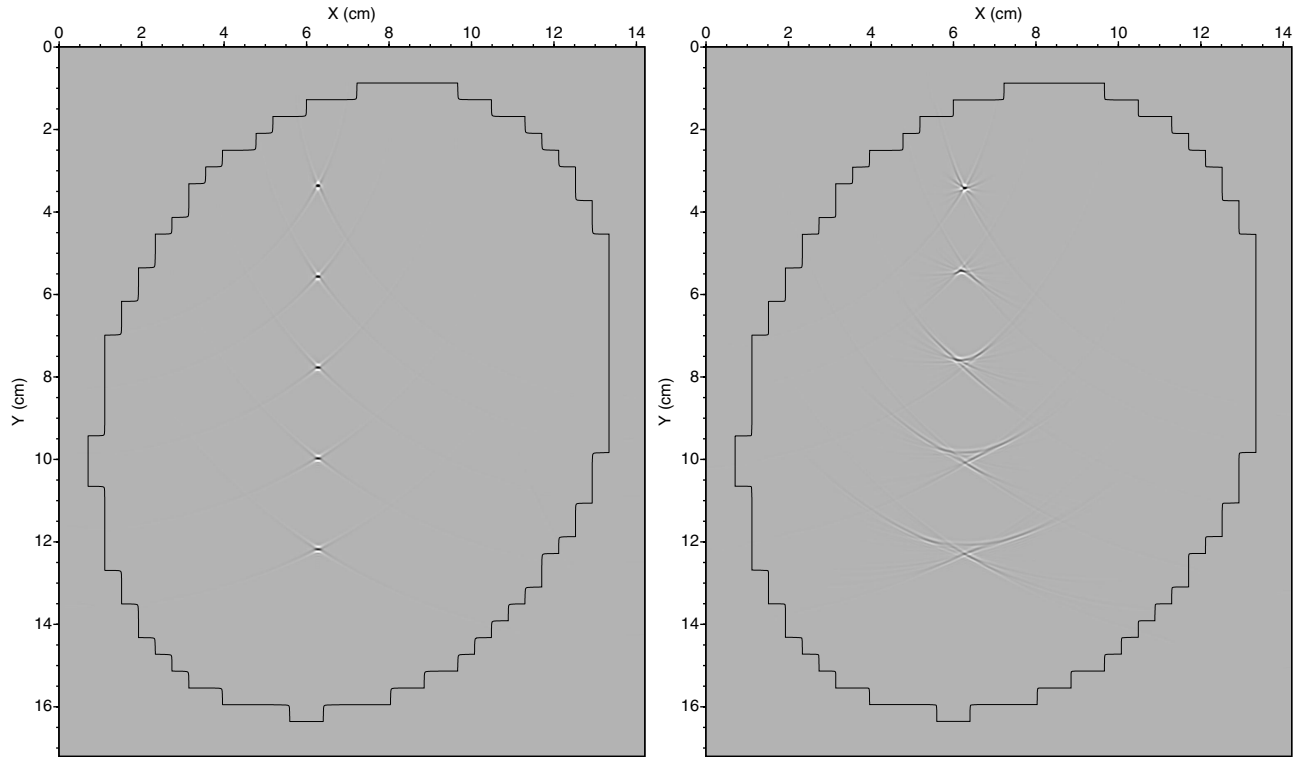

Figure 10. Comparison of images of the five point sources reconstructed using the same data along the top boundary of the breast model but different sound-speed models. (a) is the image obtained using the correct breast sound-speed model shown in Figure 1(a). (b) is the image obtained using the average sound-speed of the breast as displayed in Figure 1(b), showing that significant image artifacts are produced, particularly for deeper imaging objects.

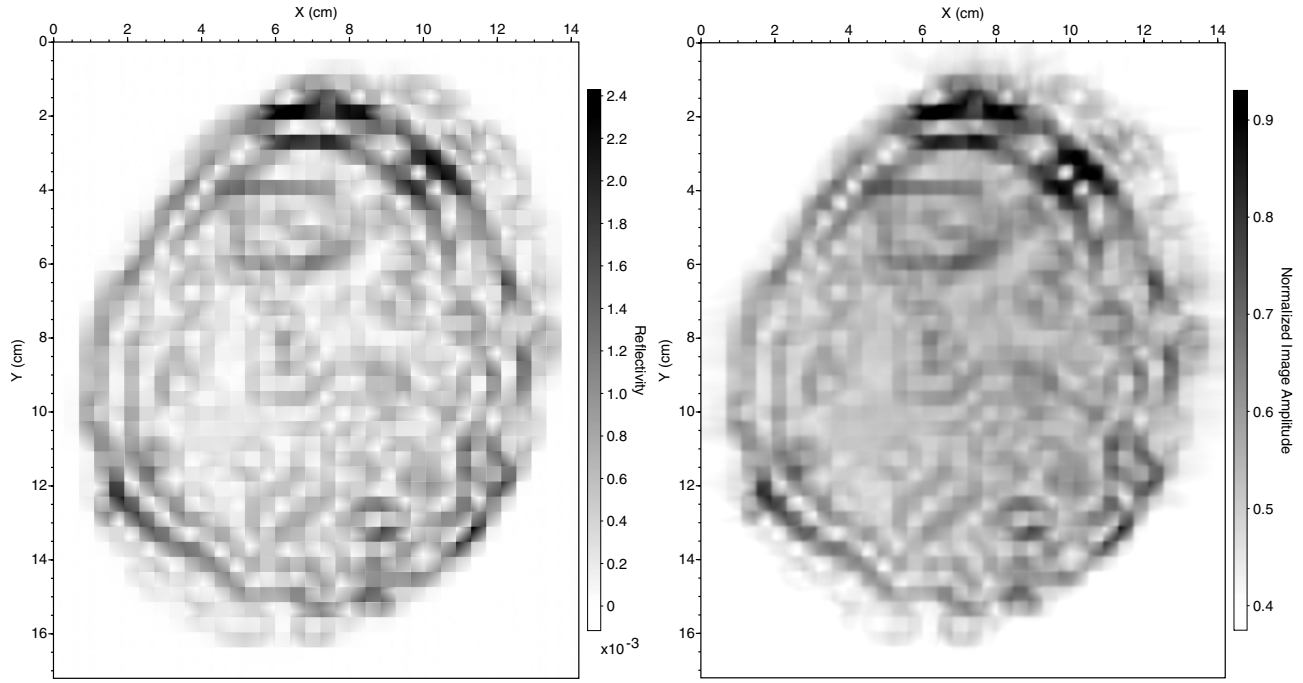

(a) Reflectivity (b) Imaging result

Figure 11. (a) Reflectivity of the breast sound-speed model shown in Figure 1(a) that was bilinearly interpolated from a preliminary transmission tomographic result produced using a large grid spacing of 4.072 mm. (b) Reconstructed image of the breast using full-aperture data of synthetic time-reversal-induced ultrasound, accurately showing locations where changes of the breast sound-speeds occur. A finer grid spacing of the breast model is needed to obtain better image resolution.

5. IMAGING WITH DIFFERENT LENGTHS OF LINEAR TRANSDUCER ARRAYS

We investigated resolution of the time-reversal imaging using linear ultrasound transducer arrays with different lengths. During the finite-difference modeling, we used a larger model than what is shown in Figure 1(a) and recorded synthetic data at a straight line of 20 cm along the top boundary of the model. The data-acquisition line was centered at the point x=6.29 cm, which is the x-position of the five point sources. We used an one-way wave-equation-based method for backpropagation of recorded ultrasonic signals during image reconstruction. Figures 8(a)-(d) are images obtained using synthetic data for linear transducer arrays with lengths of 5 cm to 20 cm, each centered at the point x=6.29 cm. When the transducer-array length is 5 cm (Figures 8a), the image resolution along x-direction is poor for targets located more than 5 cm away from the transducer array. The image resolution along x-direction increases with increasing of the length of the linear transducer array, as shown in Figures 8(b)-(d).

Figure 9 shows normalized images along x-direction for different images in Figures 8. Like Figure 7, the narrower FWHM gives better image resolution. When the imaging object is close to the transducer array as depicted in Figure 9(a), the image resolution along x-direction is similar to one another when the transducer-array lengths are longer than 10 cm. Figure 9(b) shows that, when the transducer-array length increases from 5 cm to 10 cm, the resolution of images for objects located more than 10 cm away from the transducer array improves significantly. The image resolution increases slowly when increasing the length from 10 cm to 15 cm, and even slowly from 15 cm to 20 cm. As demonstrated in Figure 9(b), when the imaging objects are more than 10 cm away from the transducer array, it is necessary to use a linear transducer array with a length longer than 15 cm in order to obtain high-resolution images.

6. IMAGING WITH A HOMOGENEOUS SOUND-SPEED MODEL

We compare images of the five point sources obtained using the correct breast sound-speed model (Figure 10a) with those obtained using the average sound-speed of the breast (Figure 10b). They were both obtained using the synthetic TR-induced data at the top boundary of the breast model and an one-way wave-equation-based backpropagation method.

Figure 10(b) demonstrates that using the average sound-speed for backpropagation of ultrasonic wavefields can only approximately image the point at y=3.39 cm, but its image have more artifacts than that in Figure 10(a). For the deeper objects, using the average sound-speed of the breast for imaging cannot correctly image them but produced a lot of image artifacts as shown in Figure 10(b). The deeper the objects are, the stronger are the image artifacts.

7. BREAST IMAGING OF A SYNTHETIC TIME-REVERSAL-INDUCED DATASET

We generated synthetic TR-induced data for the breast model shown in Figure 1(a) using a Ricker source-time function with a central frequency of 1 MZ as the source function. Ultrasonic sources were located at all discrete points within the breast model to generate TR-induced ultrasonic waves. The amplitudes of ultrasonic sources is proportional to the absolute values of reflectivity of the breast sound-speed model. The reflectivity of the breast model in Figure 1(a) is displayed in Figure 11(a). It shows that the grid spacing used in ultrasound tomography to obtain the breast sound-speed in Figure 1(a) is large (4.072 mm). A much finer grid spacing is needed to obtain better image resolution. The synthetic TR-induced ultrasonic data were generated using the finite-difference wave-equation scheme, and recorded along all boundaries of the breast model. Figure 11(b) is the image produced by the imaging method using time-reversed ultrasonic data along all boundaries of the breast model. Comparing the image in Figure 11(b) with the reflectivity of the breast model in Figure 11(a), it demonstrates that time-reversal imaging with TR-induced data can produce high-quality and high-resolution image of the breast showing locations where changes of sound speeds within the breast occur.

For applications to real data (*in-vitro* or *in-vivo* data), noise in measured ultrasonic data can affect image resolution. On the other hand, iterative TRM can improve signal to noise ratios and consequently improve image quality and resolution. We will apply our time-reversal imaging method to real TR-induced data to investigate its imaging capability.

8. CONCLUSIONS

We have developed a time-reversal imaging method by backpropagating time-reversal-induced ultrasonic signals into the breast using solutions of two-way (full) wave equation or one-way wave equation. We have shown that imaging with full-aperture data produces images with the best quality and highest resolution. When imaging with limited-aperture data (or data from a linear ultrasound transducer array), we found that the one-way wave-equation-based imaging method produces higher-resolution images than the two-way wave-equation-based imaging method. In addition, one-way wave-equation-based imaging is more than 15 times faster than two-way wave-equation-based imaging. A relative long linear transducer array must be used in order to obtain high-resolution images of deeper targets. In general, the length of a linear transducer array must be longer than the distance between the transducer array and imaging objects. We have demonstrated that imaging with an average sound-speed model of the breast can produce significant image artifacts, particular for deep imaging objects. Our preliminary imaging examples with synthetic data have demonstrated that imaging with time-reversed ultrasound can produce high-quality and high-resolution images of the breast. This appears to have substantial clinical implications in the future for improving image resolution and contrast, leading to improved detection of tumor margins and possible localization of many more microcalcifications.

ACKNOWLEDGMENT

This work was supported through the DOE Laboratory-Directed Research and Development program at Los Alamos National Laboratory.

REFERENCES

1. J. F. Greenleaf, A. Johnson, R. C. Bahn, and B. Rajagopalan, "Quantitative cross-sectional imaging of ultrasound parameters," in *1977 Ultrasonics Symposium Proceedings*, IEEE, pp. 989–995, 1977.
2. S. J. Norton and M. Linzer, "Ultrasonic reflectivity tomography: reconstruction with circular transducer arrays," *Ultrasonic Imaging* **2**, pp. 154–184, 1979.
3. P. L. Carson, C. R. Meyer, A. L. Scherzinger, and T. V. Oughton, "Breast imaging in coronal planes with simultaneous pulse echo and transmission ultrasound," *Science* **214**, pp. 1141–1143, 1981.
4. M. P. Andre, H. S. Janee, P. J. Martin, G. P. Otto, B. A. Spivey, and D. A. Palmer, "High-speed data acquisition in a diffraction tomography system employing large-scale toroidal arrays," *International Journal of Imaging Systems and Technology* **8**, pp. 137–147, 1997.

5. S. A. Johnson, D. T. Borup, J. W. Wiskin, F. Natterer, F. Wuebbling, Y. Zhang, and O. C., "Apparatus and method for imaging with wavefields using inverse scattering techniques," *United States Patent* **6,005,916**, 1999.
6. V. Z. Marmarelis, T. S. Kim, and R. E. N. Shehada, "High resolution ultrasonic transmission tomography," in *Ultrasonic Imaging and Signal Processing*, W. F. Walker and M. F. Insana, eds., *Proc. SPIE* **5035**, pp. 33–40, The International Society for Optical Engineering, (Bellingham, Washington), 2002.
7. D.-L. Liu and R. C. Waag, "Propagation and backpropagation for ultrasonic wavefront design," *IEEE Trans. on Ultras. Ferro. and Freq. Contr.* **44**, pp. 1–13, 1997.
8. P. J. Littrup, N. Duric, S. Azevedo, D. H. Chambers, J. V. Candy, S. Johnson, G. Auner, J. Rather, and E. T. Holsapple, "Computerized Ultradound Risk Evaluation (CURE) system: Development of combined transmission and reflection ultrasound with new reconstruction algorithms for breast imaging," *Acoustical Imaging* **26**, pp. 175–182, 2002.
9. P. Littrup, N. Duric, R. R. Leach Jr., S. G. Azevedo, J. V. Candy, T. Moore, D. H. Chambers, J. E. Mast, and E. T. Holsapple, "Characterizing tissue with acoustic parameters derived from ultrasound data," in *Ultrasonic Imaging and Signal Proceesing*, M. Insana and W. F. Walker, eds., *Proc. SPIE* **4687**, pp. 354–361, The International Society for Optical Engineering, (Bellingham, Washington), 2002.
10. R. R. Leach Jr., S. G. Azevedo, J. G. Berryman, H. R. Bertete-Aguirre, S. H. Chambers, J. E. Mast, P. Littrup, N. Duric, S. A. Johnson, and F. Wuebbeling, "Comparison of ultrasound tomography methods in circular geometry," in *Ultrasonic Imaging and Signal Proceesing*, M. Insana and W. F. Walker, eds., *Proc. SPIE* **4687**, pp. 362–377, The International Society for Optical Engineering, (Bellingham, Washington), 2002.
11. D. H. Chambers and P. Littrup, "Ultrasound imaging using diffraction tomography in a cylindrical geometry," in *Ultrasonic Imaging and Signal Processing*, M. Insana and W. F. Walker, eds., *Proc. SPIE* **4687**, pp. 412–420, The International Society for Optical Engineering, (Bellingham, Washington), 2002.
12. N. Duric, P. Littrup, E. T. Holsapple, A. Babkin, R. Duncan, A. Kalinin, R. Pevzner, and M. Tokarev, "Ultrasound tomography of breast tissue," in *Ultrasonic Imaging and Signal Processing*, W. F. Walker and M. Insana, eds., *Proc. SPIE* **5035**, The International Society for Optical Engineering, (Bellingham, Washington), 2003.
13. L. Huang, N. Duric, and P. Littrup, "Ultrasonic breast imaging using a wave-equation migration method," in *Ultrasonic Imaging and Signal Processing*, W. F. Walker and M. Insana, eds., *Proc. SPIE* **5035**, pp. 432–439, The International Society for Optical Engineering, (Bellingham, Washington), 2003.
14. N. Duric, P. J. Littrup, A. Babkin, D. Chambers, S. Azevedo, A. Kalinin, R. Pevzner, M. Tokarev, E. Holsapple, O. Rama, and R. Duncan, "Development of ultrasound tomography for breast imaging: Technical assessment," *Medical Physics* **32**, pp. 1375–1386, 2005.
15. N. Duric, P. J. Littrup, O. Rama, and E. T. Holsapple, "Computerized ultrasound risk evaluation (CURE): First clinical results," *Acoustical Imaging* **28**, 2005 (in press).
16. M. Fink, "Time-reversal mirrors," *J. Phys. O: Appl. Phys.* **26**, pp. 1333–1350, 1993.
17. S. Yon, M. Tanter, and M. Fink, "Sound focusing in rooms: The time-reversal approach," *Journal of the Acoustical Society of America* **113**, pp. 1533–1543, 2003.
18. M. Heinemann, A. Larraza, and K. Smith, "Experimental studies of applications of time-reversal acoustics to noncoherent underwater communications," *ournal of the Acoustical Society of America* **113**, pp. 3111–3116, 2003.
19. N. Chakroun, M. A. Fink, and F. Wu, "Time reversal processing in ultrasonic nondestructive testing," *IEEE Transactions on Ultrasonics, Ferroelectrics and Frequency Control* **42**, pp. 1087–1098, 1995.
20. C. Prada, E. Kerbrat, D. Cassereau, and M. Fink, "Time reversal techniques in ultrasonic nondestructive testing of scattering media," *Inverse Problems* **18**, pp. 1761–1773, 2002.
21. M. Fink, G. Montaldo, and M. Tanter, "Time-reversal acoustics in biomedical engineering," *Annu. Rev. Biomed. Eng.* **5**, pp. 465–497, 2003.
22. M. Fink, "Time reversed acoustics," *Physics Today* **50**, pp. 34–40, 1997.
23. M. Fink, "Time reversed acoustics," in *Review of Progress in Quantitative Nondestructive Evaluation*, D. O. Thompson and D. E. Chimenti, eds., **20**, pp. 1–15, American Institute of Physics, 2001.
24. J. F. Claerbout, *Imaging the Earth's Interior*, Blackwell Scientific Publications, Oxford, 1985.
25. O. Holberg, "Computational aspects of the choice of operator and sampling interval for numerical differentiation in large-scale simulation of wave phenomena," *Geophys. Prosp.* **35**, pp. 629–655, 1987.
26. R. L. Higdon, "Absorbing boundary conditions for elastic waves," *Geophysics* **56**, pp. 231–241, 1991.
27. L. Huang and M. C. Fehler, "Globally optimized Fourier finite-difference migration method," in *Expanded Abstracts*, pp. 802–805, 70th Ann. Internat. Mtg., Soc. Expl. Geophys., (Calgary, Canada), 2000.